IPA: An Information-Reconstructive Input Projection Framework for Efficient Foundation Model Adaptation

Yuan Yin *yuan.yin@valeo.com*
Valeo.ai, Paris, France

Shashanka Venkataramanan *shashanka.venkataramanan@valeo.com*
Valeo.ai, Paris, France

Tuan-Hung Vu *tuan-hung.vu@valeo.com*
Valeo.ai, Paris, France

Andrei Bursuc *andrei.bursuc@valeo.com*
Valeo.ai, Paris, France

Matthieu Cord *matthieu.cord@valeo.com*
Valeo.ai, Paris, France
Sorbonne Université, CNRS, ISIR, F-75005 Paris, France

Reviewed on OpenReview: *https://openreview.net/forum?id=aLmQeZx2pR*

Abstract

Parameter-efficient fine-tuning (PEFT) methods, such as LoRA, reduce adaptation cost by injecting low-rank updates into pretrained weights. However, LoRA's down-projection is randomly initialized and data-agnostic, discarding potentially useful information. Prior analyses show that this projection changes little during training, while the up-projection carries most of the adaptation, making the random input compression a performance bottleneck. We propose IPA, a feature-aware projection framework that explicitly aims to reconstruct the original input within a reduced hidden space. In the linear case, we instantiate IPA with algorithms approximating top principal components, enabling efficient projector pretraining with negligible inference overhead. Across language and vision benchmarks, IPA consistently improves over LoRA and DoRA, achieving on average 1.5 points higher accuracy on commonsense reasoning and 2.3 points on VTAB-1k, while matching full LoRA performance with roughly half the trainable parameters when the projection is frozen. Code available at https://github.com/valeoai/peft-ipa.

1 Introduction

Foundation models have transformed machine learning research and applications with their broad capabilities in language and visual understanding. These capabilities arise from model scale, since models with billions of parameters are pre-trained on massive corpora (Bommasani et al., 2021). However, adapting such general-purpose models to specialized tasks or domains remains challenging: as model sizes grow, full fine-tuning becomes computationally and financially expensive (Houlsby et al., 2019; Hu et al., 2022).

To address this bottleneck, the community has developed a range of parameter-efficient fine-tuning (PEFT) methods that reduce the number of trainable parameters by an order of magnitude compared to the base model (see surveys, e.g., Han et al., 2024; Zhang et al., 2025). Among these, Low-Rank Adaptation (LoRA; Hu et al., 2022) has gained significant traction due to its simplicity and effectiveness in the large-language-model community. In LoRA, each target weight matrix is reparameterized as the sum of the original pre-trained weight W and a low-rank update $\Delta W = BA$, where A (the "down" projection) maps inputs into a lower-dimensional space and B (the "up" projection) maps them back to the output dimension. This additional module can be merged into W without introducing any extra latency during inference.

Although there has been a flurry of follow-up works around LoRA, most focus on alternative initializations (Meng et al., 2024; Yang et al., 2024) or extended structures (Liu et al., 2024; Huang et al., 2025; Albert et al., 2025) by restricting their analysis to the pretrained weight matrix, while paying little attention to the distribution of input features. In contrast, we broaden the focus to explicitly account for the role of input features.

In the original LoRA formulation, the down-projection matrix A is randomly initialized and thus data-agnostic. Analyses of LoRA's inherent asymmetry show that during adaptation, this down-projection A remains close to its initialization, whereas the up-projection B adapts more effectively to the data (Tian et al., 2024; Hayou et al., 2024b; Zhu et al., 2024). This suggests that a data-agnostic input projection can become a performance bottleneck, motivating its replacement with a feature-aware, data-dependent alternative that better aligns with the intrinsic structure of the inputs.

In this paper, we tackle this direction and introduce IPA, an input-feature-aware projection scheme that preserves optimally the input information in the reduced hidden feature space. Our contributions are:

- We formulate adaptation with a dedicated feature-projection pretraining objective that favors information reconstruction in the bottleneck dimension through an encoder-decoder formulation.
- We instantiate this framework in the linear setting using efficient forward-only pretraining algorithms.
- We empirically validate IPA on language and vision-language tasks, showing consistent improvements over random linear projections. On several architectures, IPA matches the performance of fully trained LoRA while requiring roughly half as many trainable parameters.

2 Related Work

Parameter efficient adapters. PEFT techniques address the high computational cost of fine-tuning large foundational models by updating only a small set of parameters, rather than the full original network. A prominent class of PEFT methods is adapter-based: small trainable modules are added to a frozen model. Early work inserted bottleneck adapters between layers to enable task-specific tuning without altering original weights (Houlsby et al., 2019; Rebuffi et al., 2017); later designs placed adapters in parallel to existing layers for improved adaptation (He et al., 2022a). Recent work have explored structured parameterizations, e.g., Kronecker-factored matrices (Mahabadi et al., 2021). Li et al. (2024) employ block-specific adapter designs, dynamic parameter sharing, and mixtures of experts to improve efficiency and generalization. At the matrix level, LoRA and its variants constrain weight updates to a low-dimensional subspace for memory and compute-efficient tuning (Hu et al., 2022; Liu et al., 2024). Indeed, He et al. (2022a) show that many PEFT methods can be viewed through a unified lens of adapter.

Beyond architectural modifications, other PEFT strategies focus on minimizing the number of updated weights directly. These include sparse update methods (Guo et al., 2021; Sung et al., 2021; He et al., 2022b), which identify and tune only the most critical parameters. Recent work has even explored extremely low-precision adapters through quantization (Jie et al., 2023), demonstrating that 1-bit adapters can rival or surpass other PEFT strategies in both parameter efficiency and performance.

LoRA methods and insights. Among PEFT techniques, LoRA-based methods have emerged as particularly prominent due to their simplicity, inspiring a wide range of follow-up studies.

Several works aim to improve LoRA's design. Some focus on alternative initialization schemes. PiSSA (Meng et al., 2024) and CorDA (Yang et al., 2024) leverage spectral decompositions of the pretrained weights to initialize LoRA modules more effectively. Shuttleworth et al. (2024) observe that LoRA introduces novel singular directions absent in full fine-tuning. Building on this, LoRA-Null (Tang et al., 2025) initializes adapters in the nullspace of pretrained activations to reduce forgetting. Other approaches propose architectural modifications. DoRA (Liu et al., 2024) decomposes pretrained weights into basis and scaling components and applies LoRA on the basis. VeRA (Kopiczko et al., 2024) further simplifies this by fixing both A and B to random bases and learning only scaling coefficients. RandLoRA (Albert et al., 2025) aggregates multiple VeRA-like components to achieve higher-rank updates. HiRA (Huang et al., 2025) follows a different route, applying element-wise multiplication between the LoRA module and the pretrained weight. These methods are all motivated by structural properties of the pretrained weights.

A parallel line of work investigates LoRA's learning behavior. Hayou et al. (2024b;a) analyze how imbalanced initialization affects feature-level dynamics during training. Zhu et al. (2024) report an asymmetry between the down- and up-projection matrices induced by standard initialization, which motivates subsequent variants such as HydraLoRA (Tian et al., 2024) and MALoRA (Wang et al., 2025). We refer the reader to Mao et al. (2025); Han et al. (2024) for more comprehensive overviews of LoRA and its many variants.

Our method differs from prior architectural improvements in that it also analyzes the input features to the target layers, rather than focusing solely on the pretrained weights. Drawing inspiration from studies on LoRA's learning behavior, our approach introduces a feature-aware projection objective that optimally preserves information in the input representation before applying the low-rank update.

3 IPA: Information-Reconstructive Input Projection for Adaptation

In this section, we begin by motivating the framework through empirical observations of standard LoRA training (Sections 3.1 and 3.2). Next, we present the IPA framework (Section 3.3), and finally provide a concrete instantiation (Section 3.4), which we evaluate in Section 4.

3.1 Preliminaries: LoRA

LoRA adapts a pretrained transformer-based model to a downstream task defined by a loss function $\mathcal{L}$ over a dataset $\mathcal{D}$. The pretrained model contains K weight matrices denoted by $\{W^{(\ell)}\}_{\ell=1}^{K}$. For simplicity, we omit the layer index ℓ when not required. Each pretrained weight matrix $W \in \mathbb{R}^{d_{\text{out}} \times d_{\text{in}}}$ defines a linear map $f_W : x \in \mathbb{R}^{d_{\text{in}}} \mapsto z = Wx \in \mathbb{R}^{d_{\text{out}}}$, which transforms an input feature vector x into an output feature vector z. Here, d_{in} and d_{out} denote the input and output dimensions of the layer, respectively.

To adapt a target layer, this linear map f_W is augmented with two additional learnable maps: $f_A : x \in \mathbb{R}^{d_{\text{in}}} \mapsto x_h = Ax \in \mathbb{R}^r, f_B : x_h \in \mathbb{R}^r \mapsto Bx_h \in \mathbb{R}^{d_{\text{out}}}$, where $A \in \mathbb{R}^{r \times d_{\text{in}}}$ and $B \in \mathbb{R}^{d_{\text{out}} \times r}$ are low-rank matrices with a maximum rank $r \ll \max(d_{\text{in}}, d_{\text{out}})$. x_h is the hidden feature projected by the mapping f_A. Adaptation proceeds over T steps of gradient descent, with $t = 0$ denoting the initial state. We denote the matrices at step t by A_t and B_t. The modified forward pass of each target layer becomes

$$z = f_W(x) + \lambda f_{B_t}(f_{A_t}(x)) = Wx + \lambda B_t A_t x, \tag{1}$$

The elements of A_0 are drawn from a zero-mean Gaussian (or uniform) distribution and $B_0 = 0$, ensuring $W + B_0 A_0 = W$ while remaining trainable. The pretrained matrix W remains frozen, and the positive scalar λ rescales the low-rank residual update. In the original LoRA formulation, $\lambda = \frac{\alpha}{r}$, where $\alpha > 0$ is a tunable hyperparameter. Training LoRA thus implies computing gradients only for A_t and B_t:

$$\nabla_{B_t}\mathcal{L} = \lambda \nabla_z \mathcal{L} x^\top {A_t}^\top, \qquad \nabla_{A_t}\mathcal{L} = \lambda {B_t}^\top \nabla_z \mathcal{L} x^\top, \tag{2}$$

leaving the pretrained weight unchanged.

3.2 Asymmetric Behaviors in LoRA

While LoRA has been widely adopted for efficient fine-tuning of large pretrained models, we observe a notable asymmetry between its two projection matrices: the down-projection matrix A primarily serves to compress input features into a low-dimensional subspace, whereas the up-projection matrix B plays the critical role of recombining those features to adapt the final model outputs. Notably, tuning B alone while keeping A fixed or randomly initialized often yields performance comparable to tuning both. This suggests that B is mainly responsible for adapting the output, whereas A serves as a feature projector.

To empirically illustrate this asymmetry, we conduct an adaptation experiment across multiple tasks. Following Huang et al. (2023), we choose the few-shot adaptation setting on the BIG-Bench Hard benchmark (BBH;

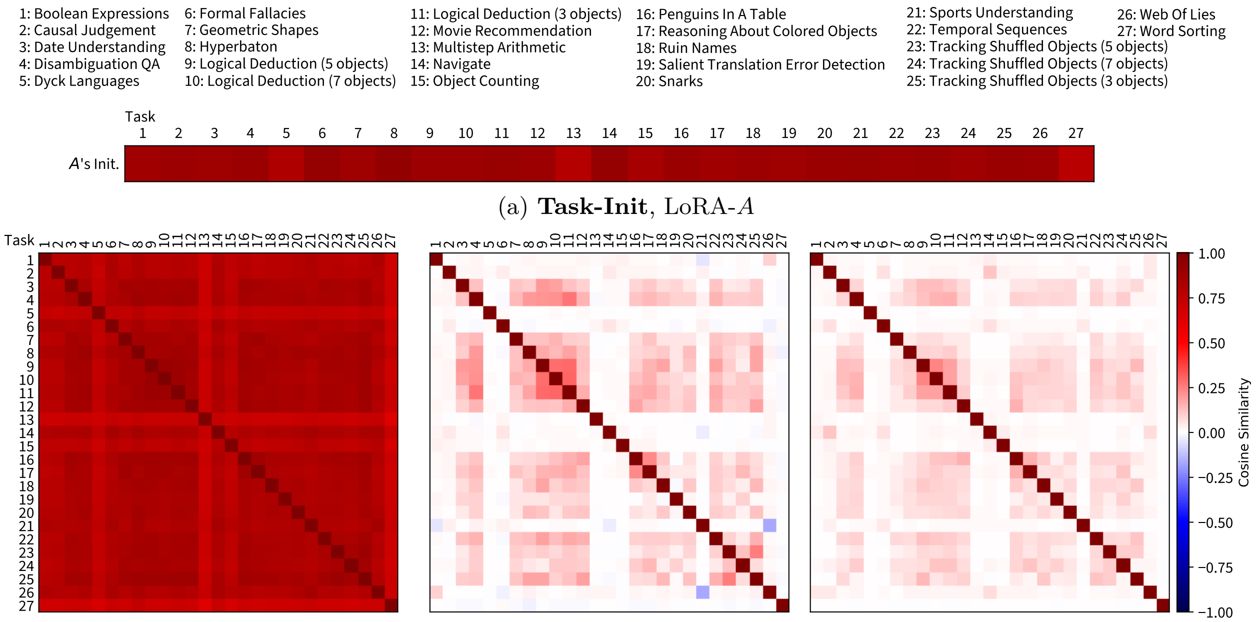

(a) **Task-Init**, LoRA-A

(b) **Task-Task**, LoRA-A

(c) **Task-Task**, LoRA-B

(d) **Task-Task**, Full FT update

Figure 1: **Cosine-similarity matrices for LoRA and full-fine-tune updates on 27 BIG-Bench Hard tasks.** (a) shows the similarity between each trained LoRA-A vector and its initialization; panels (b)–(d) show pairwise task–task similarities for LoRA-A, LoRA-B, and full fine-tune updates, respectively. The LoRA-A vectors remain close to their shared initialization in (a) and vary little across tasks in (b), while the task-dependent patterns in LoRA-B (c) closely match those from full fine-tuning (d).

Suzgun et al., 2023), which comprises 27 diverse tasks. We use Flan-T5 (Chung et al., 2024) as the base pretrained model. For each task j, we either fully fine-tune the pretrained model or learning LoRA adapters on a set of target layer Λ for a fixed number of steps T, reaching zero training loss in both cases. All LoRA adapters are initialized with the same random seed across tasks, ensuring that $A_{0,j}^{(\ell)} = A_0^{(\ell)}$ for every target layer $\ell \in \Lambda$. This facilitates comparison of the learned LoRA matrices across tasks.

To analyze inter-task similarity, across all target layers Λ, we flatten and concatenate full-fine-tune updates and the trained LoRA matrices, yielding vectors for each task j: $\theta_{A,j} = \Vert_{\ell\in\Lambda} \operatorname{vec}\big(A_{T,j}^{(\ell)}\big)$, $\theta_{B,j} = \Vert_{\ell\in\Lambda} \operatorname{vec}\big(B_{T,j}^{(\ell)}\big)$, and $\Delta\theta_{W,j} = \Vert_{\ell\in\Lambda} \operatorname{vec}\big(W_{T,j}^{(\ell)} - W^{(\ell)}\big)$. Figure 1 then presents cosine-similarity matrices for two cases: in panel (a) ("Task–Init, LoRA-A") we compare each trained vector $\theta_{A,j}$ to their common LoRA-A initialization; panels (b)–(d) ("Task–Task, LoRA-A", LoRA-B and Full FT, respectively) show pairwise similarities $\cos(\theta_{A,i}, \theta_{A,j})$, $\cos(\theta_{B,i}, \theta_{B,j})$, and $\cos(\Delta\theta_{W,i}, \Delta\theta_{W,j})$.

Remarkably, Figure 1a shows that A matrices are still pretty similar to their initialization, while Figure 1b is largely uniform across tasks. This indicates that the learned A matrices undergo little change during adaptation and capture minimal task-dependent variation. In contrast, Figures 1c and 1d reveal nearly identical block structures, suggesting that the task-specific information recovered by full fine-tuning is almost entirely absorbed by the B matrices.

Implications. These findings indicate that the down-projection matrix A in vanilla LoRA operates primarily as a random feature projector, rather than encodes the task-specific distinctions. Recent theoretical and empirical studies of LoRA (Hayou et al., 2024b; Zhu et al., 2024; Tian et al., 2024; Zhang et al., 2025) arrive at similar conclusions, showing that standard LoRA initialization induces pronounced asymmetries in both learning dynamics and representational behavior. Consequently, replacing this random feature projector with a more expressive, task-aware mapping could yield richer intermediate representations and improve adaptation performance.

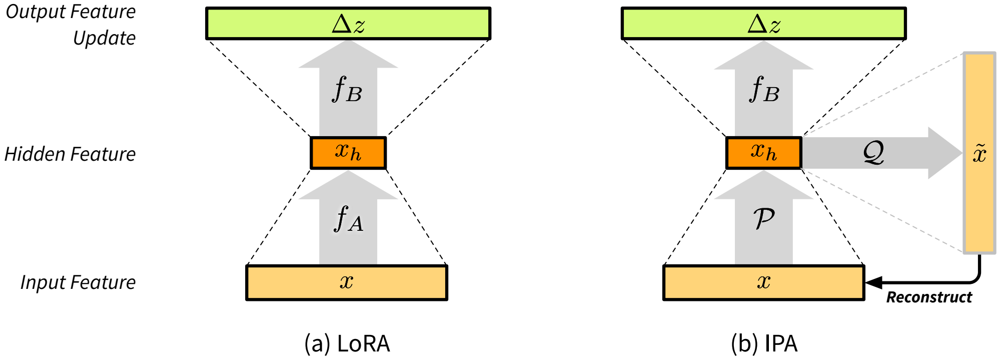

Figure 2: **Schematic of IPA vs. standard LoRA.** The gray arrows denote mappings between two vector feature spaces. In standard LoRA, an input feature x is projected to a low-dimensional space by f_A and then lifted back by f_B to yield the update Δz. IPA introduces two pretrained projectors, $\mathcal{P}$ and $\mathcal{Q}$, enforcing that the hidden feature can reconstruct x; at adaptation time only $\mathcal{P}$ is retained.

3.3 The IPA Framework

We reinterpret the adaptation scheme by introducing a general feature projection function $\mathcal{P}\colon \mathbb{R}^{d_{\text{in}}} \to \mathbb{R}^{d_h}$ and write

$$z = f_W(x) + \lambda f_{B_t}(\mathcal{P}(x)) = Wx + \lambda B_t \mathcal{P}(x), \quad B_0 = 0.$$

where $\mathcal{P}$ maps the input x into a hidden feature $x_h = \mathcal{P}(x) \in \mathbb{R}^{d_h}$. Therefore, full fine-tuning corresponds to $\mathcal{P}$ being the identity. It is thus natural to seek a closer approximation to full fine-tuning through more effective input compression.

Information-reconstructive input projection. When $d_h < d_{\text{in}}$, the projection $\mathcal{P}$ must compress x, which risks discarding task-relevant information if it is not chosen in an input-aware manner and the inputs lie in a subspace with larger intrinsic dimension. Standard LoRA initializes $\mathcal{P}$ as a random linear map, thus ignoring the input distribution. To address this, we instead seek $\mathcal{P}$ (and a complementary decoder $\mathcal{Q}\colon \mathbb{R}^{d_h} \to \mathbb{R}^{d_{\text{in}}}$) that minimize the reconstruction error:

$$\min_{\mathcal{P},\mathcal{Q}} \mathbb{E}_{x\sim \mathrm{p}(x)} \|x - \tilde{x}\|^2, \quad \text{where} \quad \tilde{x} = \mathcal{Q}(\mathcal{P}(x)). \tag{3}$$

This objective encourages $\mathcal{P}$ to preserve as much information from the original input as possible, as measured by the L^2 reconstruction loss. Figure 2 contrasts IPA with standard LoRA, highlighting the additional optimization of the projector.

Forward-only pretraining of projector. Eq. (3) corresponds precisely to the objective of an autoencoder. One could therefore imagine training it with either linear or nonlinear functions for $\mathcal{P}$ and $\mathcal{Q}$. However, doing so for each modulated layer via backpropagation is impractical: the loss is difficult to integrate into the adapter training pipeline and incurs significant computational overhead compared to LoRA. Instead, we propose to learn the projector in a *forward-only* manner.

3.4 Instantiation: Linear Case

To instantiate the framework in practice, we must specify (i) the distribution of features used to pretrain the projector $\mathcal{P}$, (ii) the form of the projector $\mathcal{P}$, and (iii) the algorithm used to pretrain it.

Pretraining distribution. We pretrain $\mathcal{P}$ using target-domain hidden representations. Concretely, we pass training tokens through the frozen pretrained model and collect the resulting hidden states, forming a pretraining set $\hat{X} = [\hat{x}_i]_{i=1}^N \in \mathbb{R}^{N\times d_{\text{in}}}$. This ensures that $\hat{X}$ reflects both the model's internal feature and the target-domain data distributions.

Projector architecture. To preserve LoRA's inference-time efficiency, we restrict $\mathcal{P}$ and its decoder $\mathcal{Q}$ to linear maps defined by a shared matrix $U \in \mathbb{R}^{d_h \times d_{\text{in}}}$:

$$\mathcal{P}(x) = Ux, \qquad \mathcal{Q}(x_h) = U^\top x_h.$$

In this setting, solving Eq. (3) is equivalent to performing PCA (Hotelling, 1933), by extracting the top-d_h eigenvectors of the empirical covariance $\Sigma = \frac{1}{N}\hat{X}^\top \hat{X}$.

Pretraining algorithm. Full PCA over all hidden states is infeasible due to storage and compute costs. Instead, we adopt incremental PCA (IPCA; Ross et al., 2008), which processes feature mini-batches sequentially and updates a low-rank approximation of Σ. Alternatives such as the generalized Hebbian algorithm (GHA; Sanger, 1989) also approximate principal components, but we found IPCA both more efficient and slightly more accurate in practice (see Section 4.4 for the ablation study).

Default Configuration. Unless otherwise specified, we use target-domain hidden representations as input, a linear projector, and IPCA for pretraining. All main experiments adopt IPCA, and IPA refers to this implementation unless noted otherwise. The projector U can optionally be refined by backpropagating the task loss, allowing it to adapt jointly with the residual weights and align more closely with the downstream objective. We analyze the effect of projector fine-tuning in Section 4.

4 Experiments

We evaluate IPA on both standard language- and vision-centric benchmarks, comparing it with leading PEFT baselines that rely on low-rank updates.

4.1 Experimental Setting

4.1.1 Tasks, Datasets, Base Models, and Evaluation Protocol

Language Tasks: Instruction Following We follow the adaptation protocol for instruction following proposed by Hu et al. (2023), where the adapted model must generate a response in the expected format from a set of given options. Each question is wrapped in a predefined natural language template with an instruction, and the training example is appended with the desired answer.

We use the `commonsense-170k` dataset, which contains 170,000 examples drawn from eight commonsense reasoning tasks. We study four recent strong pretrained large language models of moderate size: Llama-2 7B (Touvron et al., 2023), Llama-3 8B (Grattafiori et al., 2024), Qwen-2.5 7B (Qwen et al., 2024), and Gemma-3 4B (Gemma Team et al., 2025). We only use the language model part if the model is multi-modal. All models are adapted once with the same dataset for 3 epochs and evaluated on the corresponding test splits for each reasoning task.

Vision Tasks: Open-Vocabulary Image Classification We assess our method on open-vocabulary classification using the VTAB-1k benchmark (Zhai et al., 2019), which includes 19 tasks/datasets categorized into three groups: Natural, Specialized, and Structured. VTAB-1k uses exactly 1000 labeled examples per task for adaptation; the original test splits remain unchanged.[1]

We use the base variant of SigLIP-2 (Tschannen et al., 2025) as the pretrained vision-language model. For each class, we construct a text embedding by inserting the class name into the prompt "`a photo of a [CLASSNAME]`" and encoding it with the model's text encoder. All embeddings are padded to the model's maximum sequence length. This prompt formulation is fixed across methods and orthogonal to the PEFT approach.

We adapt *only the vision encoder*, training it with a standard cross-entropy loss over logits computed with similarity scores between image and text embeddings. Logits are computed following the procedure used in

[1] We regenerated VTAB-1k using the code provided in Zhang et al. (2022), converting all examples to a lossless format instead of the lossy JPEG compression used in the original work. After this change, our zero-shot test performance for SigLIP-2 matches the results reported in the model's original paper.

SigLIP-2, for each image-class pair. Adaptation and evaluation are performed independently for each task. As in Zhang et al. (2022), we evaluate models every 10 epochs and report the best test performance observed over 100 training epochs.

4.1.2 Main Baselines

Our goal is to isolate and quantify the effect of the input projector introduced in IPA, w.r.t. random input projector-based methods. We therefore compare against two strong baselines from the same reparameterization PEFT family: • **LoRA** (Hu et al., 2022), which injects a low-rank residual update with a randomly initialized down-projection f_A. • **DoRA** (Liu et al., 2024), which decomposes each pretrained weight into a magnitude and direction: $W = \|W\| \cdot \frac{W}{\|W\|}$, where $\|W\|$ is the magnitude and $\frac{W}{\|W\|}$ is the unit-norm direction. Standard LoRA is then applied only to the direction, while the magnitude $\|W\|$ is fine-tuned jointly. For each method we evaluate two variants of the input projector: fixed (no gradient updates, denoted ✗) and trainable (fine-tuned during adaptation, denoted ✓), aligning with IPA's variants.

4.1.3 Hyperparameters

Optimization. To ensure a fair comparison across adaptation methods, we fixed the optimizer hyperparameters and learning rate scheduler in all experiments except the base learning rate. We employ Adam (Kingma & Ba, 2015) with a linear warm-up schedule: the learning rate is ramped up over the first steps, then decayed linearly. The base learning rate remains unchanged regardless of whether feature-projection fine-tuning is enabled. The same batch size is applied in each benchmark.

For each baseline, we align the recommended learning rates for baselines with those from Liu et al. (2024) for Llama-2 and Llama-3. We only deviate from these defaults when a more effective rate is identified. We choose a performing learning rate for more recent Qwen-2.5 7B and Gemma-3 4B.

We report the detailed hyperparameters in Appendix A.

Adapter configuration. All methods share identical essential adapter settings to isolate differences coming solely from feature projection. Concretely, for language benchmark, we use identical hidden dimension $d_h = 32$ for the query, key, and value projections, as well as for the up/down projections in each MLP block, following Hu et al. (2023); Liu et al. (2024). For vision benchmarks, we restrict adapters to the query/value projections with $d_h = 8$, per standard practice in vision transformers as in Zhang et al. (2022). Therefore, the only methodological distinction lies in how feature projectors are trained. The scaling factor is fixed for all methods.

For instruction-following tasks, IPA uses a random 10% subset of the training data to construct the projector pretraining feature set. An ablation study examining the impact of this choice is presented in Figure 4b. For open-vocabulary classification, we leverage the full training set for each task, as each contains only 1000 examples.

4.2 Main Results

IPA projector improves performance over random projection. Tables 1 and 2 summarize our accuracy results on the instruction-following benchmark and the open-vocabulary classification tasks, respectively.

On the instruction-following benchmark at hidden dimension $d_h = 32$, IPA outperforms both LoRA and DoRA across most configurations and base models. For example, in Table 1, on Llama-3 8B without projector fine-tuning (25M trainable parameters, 0.31% of the model), IPA achieves an average accuracy of 85.6%, outperforming LoRA (85.0%) by 0.6 points and DoRA (84.7%) by 0.9 points. Even with projector fine-tuning (57M parameters, 0.70%), IPA still leads with 85.9%, compared to 85.5% for LoRA and 85.1% for DoRA. Similar gains are observed across other base models, yielding an average gain of 1.5 points.

On the open-vocabulary classification benchmark (Table 2), at hidden dimension $d_h = 8$, IPA reaches 73.7% group-level macro average accuracy without projector fine-tuning, surpassing LoRA by 3.0 points and DoRA by 2.8 points. With projector fine-tuning, performance improves to 76.5%, a 1.8-point gain over both baselines.

Table 1: **Comparison of instruction-following answer accuracy (%) on 8 commonsense reasoning benchmarks across multiple base models.** All methods are compared in the configuration with (✓) and without (✗) projector finetuning. We highlight the **best** and the second best scores under the same projector finetuning setting.

Base model	Method	Proj. FT	Trainable Params (%)	BoolQ	PIQA	SocialIQA	HellaSwag	WinoGrande	ARC-easy	ARC-challenge	OpenbookQA	Avg.
Llama-2 7B	LoRA	✗	28.0M (0.41%)	60.5	78.7	74.5	76.3	75.1	82.8	66.1	76.8	73.8
	DoRA		28.9M (0.43%)	58.0	82.0	33.5	12.8	42.1	64.9	43.9	68.4	50.7
	IPA (Ours)		28.0M (0.41%)	**71.7**	**83.2**	**80.0**	**89.0**	**82.0**	**84.8**	**70.1**	**79.0**	**80.0**
	LoRA	✓	56.1M (0.83%)	69.8	79.9	79.5	83.6	82.6	79.8	64.7	81.0	77.6
	DoRA		57.0M (0.84%)	**71.8**	83.7	76.0	89.1	82.6	83.7	68.2	**82.4**	79.7
	IPA (Ours)		56.1M (0.83%)	71.1	**84.4**	**80.9**	**90.5**	**82.7**	**85.6**	**71.5**	81.4	**81.1**
Llama-3 8B	LoRA	✗	25.2M (0.31%)	73.6	88.1	80.3	95.0	85.2	90.4	**80.1**	87.4	85.0
	DoRA		26.0M (0.32%)	74.3	87.9	79.7	95.3	84.2	90.3	79.5	86.2	84.7
	IPA (Ours)		25.2M (0.31%)	**74.8**	**88.6**	**81.1**	**95.4**	**85.6**	**91.7**	79.9	**87.8**	**85.6**
	LoRA	✓	56.6M (0.70%)	**75.4**	88.6	80.7	95.4	**86.2**	**91.2**	**80.1**	86.1	85.5
	DoRA		57.4M (0.71%)	75.3	89.3	80.8	95.3	85.8	89.9	79.3	85.6	85.1
	IPA (Ours)		56.6M (0.70%)	75.0	**89.9**	**81.2**	**96.0**	85.9	**91.2**	79.6	**88.4**	**85.9**
Qwen-2.5 7B	LoRA	✗	24.3M (0.32%)	62.8	89.3	79.9	94.6	83.1	95.9	88.6	91.4	85.7
	DoRA		25.1M (0.33%)	62.0	89.8	78.6	94.6	83.0	**96.1**	**88.9**	89.8	85.3
	IPA (Ours)		24.3M (0.32%)	**73.3**	**90.0**	**80.2**	**95.0**	**85.2**	95.8	88.8	**92.4**	**87.6**
	LoRA	✓	54.1M (0.71%)	63.5	89.8	79.5	**95.4**	**85.9**	95.9	88.3	**92.2**	86.3
	DoRA		54.9M (0.72%)	**74.5**	**90.0**	**80.2**	**95.4**	**85.9**	95.7	87.7	91.8	87.6
	IPA (Ours)		54.1M (0.71%)	**74.5**	**90.0**	79.7	95.3	85.5	**96.2**	**88.7**	92.0	**87.7**
Gemma-3 4B	LoRA	✗	21.4M (0.49%)	**69.3**	84.4	78.2	90.6	80.3	89.5	76.4	82.0	81.3
	DoRA		22.0M (0.51%)	69.1	84.2	77.9	**91.0**	80.5	89.4	**78.1**	82.2	81.5
	IPA (Ours)		21.4M (0.49%)	68.7	**85.0**	**78.5**	90.0	**81.5**	**90.3**	78.0	**84.4**	**82.0**
	LoRA	✓	46.6M (1.07%)	70.3	86.0	79.7	93.1	82.3	89.7	79.7	84.4	83.1
	DoRA		47.3M (1.09%)	**70.6**	85.3	**80.0**	92.9	82.8	90.0	77.6	85.4	83.1
	IPA (Ours)		46.6M (1.07%)	69.8	**86.3**	78.8	**93.4**	**83.3**	**90.7**	**80.3**	**86.0**	**83.6**

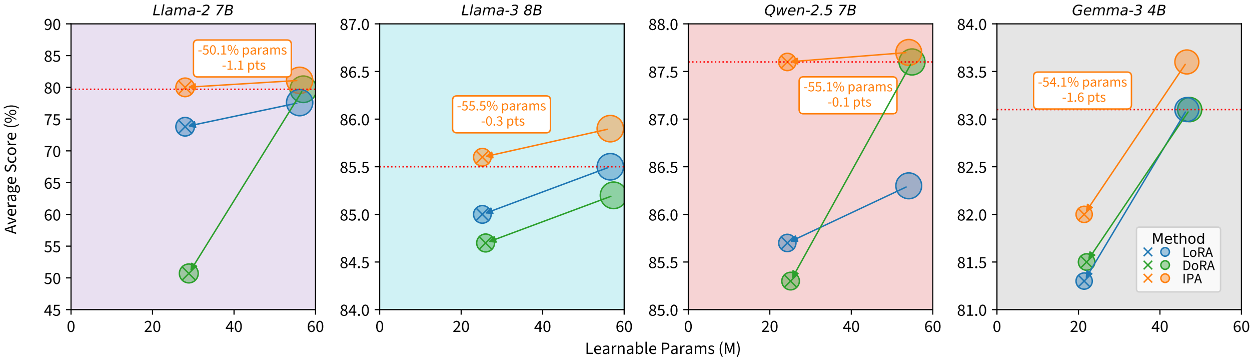

Figure 3: Comparison of IPA with baselines in both settings, with (◯) and without (⊗) finetunable feature projection on the commonsense benchmark. The dotted red line marks the highest baseline performance.

We also note that, across both benchmarks, LoRA remains competitive with DoRA, as the two methods yield similar scores in most settings when the learning rates are aligned.

IPA suffers less from fixing input projectors. The performance degradation from fixing the input projectors appears to be less pronounced for IPA in several cases. We showcase this in Figure 3. For instance, with Llama-2 7B, fixing the IPA projectors results in only a 1.1-point drop, compared to 3.8 points for

Table 2: **Top-1 accuracy (%) on 19 VTAB-1k open-vocabulary classification tasks with the SigLIP-2 base model.** Methods are evaluated with (✓) or without (✗) projector finetuning. “Vision QV FT” finetunes the query/value projection layers of the vision encoder, while “Vision Full FT” finetunes all its parameters. We highlight the **best** and second best scores under the same setting. We report per-group averages (“G1/G2/G3 Avg.”), the *Macro Avg.* (mean of group averages), and the *Micro Avg.* (mean over all tasks). *Significance:* for each setting (w/o and w/ projector finetuning), we run paired sign tests (two sided, $H_0\colon p = \frac{1}{2}$) comparing IPA against each baseline (LoRA, DoRA) over the 19 tasks. The “Sign p” column in a row reports the p-value for IPA vs. the method in that row (IPA rows use “—”).

			Group 1: Natural								Group 2: Specialized					Group 3: Structured											
Method	Proj. FT	Trainable Params (%)	Caltech101	CIFAR-100	DTD	Flowers102	Pets	Sun397	SVHN	G1 Avg.	Camelyon	EuroSAT	Resisc45	Retinopathy	G2 Avg.	Clevr-Count	Clevr-Dist	DMLab	KITTI-Dist	dSpr-Loc	dSpr-Ori	sNORB-Azim	sNORB-Elev	G3 Avg.	Macro Avg.	Micro Avg.	Sign p
Zero-shot		0 (0.00%)	84.4	73.9	63.0	84.1	94.9	61.2	28.6	70.0	50.9	40.0	62.8	5.0	39.7	27.9	20.0	17.0	4.2	6.4	4.8	5.2	10.4	12.0	40.5	36.7	—
Vision QV FT	—	14.2M (3.8%)	94.2	78.3	80.2	98.2	93.3	66.6	93.2	85.2	85.3	96.5	91.0	74.8	86.9	85.0	60.2	48.5	85.1	88.2	52.2	37.2	43.6	62.5	78.2	75.5	—
Vision Full FT		92.9M (24.8%)	94.8	81.5	81.3	98.3	94.7	67.7	93.2	86.1	85.0	96.3	91.5	75.1	87.0	84.1	60.8	42.8	86.1	51.5	83.0	29.7	41.8	60.0	77.7	74.7	—
LoRA		0.15M (0.039%)	89.0	81.8	75.4	94.3	95.3	64.6	89.9	84.3	79.2	**95.8**	87.0	72.5	83.7	**85.0**	52.2	26.8	71.4	65.9	17.5	8.8	24.0	43.9	70.7	66.0	0.019
DoRA	✗	0.17M (0.044%)	89.6	**82.0**	76.0	94.5	**95.4**	64.8	90.3	84.7	79.3	95.7	86.8	72.5	83.6	84.8	54.5	28.3	67.2	68.0	17.6	9.1	25.8	44.4	70.9	66.3	0.004
IPA (Ours)		0.15M (0.039%)	**93.1**	81.7	**77.7**	**95.3**	95.1	**65.2**	**90.7**	**85.5**	**81.5**	95.7	**87.3**	**73.3**	**84.5**	83.5	**59.7**	**29.2**	**81.4**	**75.0**	**25.1**	**15.8**	**38.6**	**51.0**	**73.7**	**69.5**	—
LoRA		0.29M (0.079%)	**94.8**	80.8	75.4	95.8	**95.2**	**65.6**	91.4	85.9	82.4	96.1	88.0	74.0	85.1	**91.8**	58.5	34.7	83.1	76.8	38.4	18.2	38.0	54.9	75.3	71.5	0.019
DoRA	✓	0.33M (0.083%)	94.5	81.1	78.1	95.8	**95.2**	**65.6**	91.4	85.7	**83.5**	96.0	87.6	74.1	85.3	91.5	60.6	35.3	**84.5**	78.4	35.3	17.0	37.1	55.0	75.3	71.5	0.019
IPA (Ours)		0.29M (0.079%)	**94.8**	**81.3**	**79.8**	**96.3**	94.7	**65.6**	**91.8**	**86.3**	83.0	**96.5**	**88.5**	**74.4**	**85.6**	90.0	**62.5**	**39.5**	82.1	**79.5**	**40.8**	**22.3**	**44.3**	**57.6**	**76.5**	**72.9**	—

LoRA and a substantial 29.0 points for DoRA. On Qwen-2.5 7B, the drop is only 0.1 points for IPA, versus 0.6 and 2.3 points for LoRA and DoRA, respectively.

In Figure 3, the red dashed lines indicate the average accuracy of the best baseline with projector finetuning. We observe that IPA without projector finetuning matches or exceeds this baseline in 3 out of 4 models, while using less than half the tunable parameters. For instance, on Llama-2 7B, it requires 50.1% fewer parameters yet surpasses LoRA and DoRA by 3.5 and 0.3 points, respectively. On Llama-3 8B, it achieves comparable gains with 55.5% fewer parameters, outperforming LoRA and DoRA by 0.1 and 0.5 points.

These results further underscore the benefit of our input projector’s information-preserving property.

4.3 Extended Comparison with Additional Baselines

We further broadened our evaluation on the commonsense reasoning benchmark using Llama-3 8B (cf. Section 4.1).

Method	Avg.
PiSSA	84.6
OLoRA	84.4
CorDA	80.8
RandLoRA	83.4
VeRA (r=512)	80.1
LoRA	85.5
DoRA	85.1
IPA (Ours)	**85.9**

Table 3: Comparison with additional PEFT methods.

Projection	Proj. FT	Scaling λ	Avg.
Random orthogonal	✗	0.25	81.7
Random orthogonal		$0.25\sqrt{\frac{d_{\text{in}}}{d_{\text{h}}}}$	82.2
LoRA		2	85.0
IPA (Ours)		0.25	**85.6**
Random orthogonal	✓	0.25	85.5
Random orthogonal		$0.25\sqrt{\frac{d_{\text{in}}}{d_{\text{h}}}}$	83.1
LoRA		2	85.5
IPA (Ours)		0.25	**85.9**

Table 4: Comparison of projection types on commonsense.

Comparison with additional baselines. In Table 3, we evaluated IPA against a broader set of baselines, including methods that rely on random projections such as VeRA (Kopiczko et al., 2024) and RandLoRA (Albert et al., 2025), as well as approaches based on spectral or low-rank matrix decompositions such as PiSSA (Meng et al., 2024), OLoRA (Büyükakyüz, 2024), and CorDA (Yang et al., 2024). Within this expanded set of techniques, IPA attains the highest average performance. All models use a hidden dimension $d_h = 32$, except VeRA. Additional per-task results and learning rate are provided in Table 6 in Appendix B.

Comparison with random orthogonal projection. In Table 4, we compared IPA with random orthogonal projections under matched hidden dimension ($d_h = 32$) and scaling configurations. Since random orthogonal projections reduce the norm of projected activations, we introduce an additional scaling factor to compensate for this effect and ensure a fair comparison with the norm-preserving PCA-based projection. In both scaling setups, random projection remains consistently below the performance of LoRA and IPA. See Appendix B, Table 7 for detailed results.

4.4 Ablation Studies

The following ablations also use Llama-3 8B on the instruction-following fine-tuning task.

Projector pretraining algorithm. As introduced in Section 3.4, we compare two online algorithms for estimating the top principal components: IPCA and GHA. Both optimize the same autoencoding objective Eq. (3). Table 5 reports results with and without projector fine-tuning. Across all settings, IPA-IPCA achieves higher downstream accuracy and converges more reliably than its GHA-based counterpart, making it our default choice.

Table 5: Comparison of instruction-following answer accuracy (%) between IPCA and GHA algorithms on commonsense reasoning benchmark.

Method	Proj. FT	BoolQ	PIQA	SocialIQA	HellaSwag	WinoGrande	ARC-easy	ARC-challenge	OpenbookQA	Avg.
IPA-IPCA	✗	**74.8**	**88.6**	**81.1**	**95.4**	**85.6**	**91.7**	79.9	**87.8**	**85.6**
IPA-GHA		73.3	88.1	80.3	95.0	85.1	91.0	**80.0**	87.2	85.0
IPA-IPCA	✓	**75.0**	**89.9**	81.2	**96.0**	85.9	**91.2**	79.6	**88.4**	**85.9**
IPA-GHA		74.9	89.3	**81.3**	95.8	**86.3**	90.4	**80.1**	86.2	85.6

Projector pretraining set size. The `commonsense-170k` dataset is large enough to investigate how the size of the projector pretraining set affects downstream performance. In Figure 4b, we pretrain the projector on randomly shuffled subsets ranging from 1% to 100% of the data, using a fixed seed for reproducibility. We select the first X% of examples from the shuffled split. Although performance generally improves up to around 10% of the data, we observe mitigated results beyond that point, which is likely due to variance in sample composition and/or randomized version of IPCA. Pretraining the feature projector on the full feature set takes roughly 1.7 hours on a NVIDIA H100 GPU, which is about ten times longer than using a 10% subset (≈10 minutes). Note that adapter tuning on the full dataset requires about 5 hours for 3 epochs. Despite the substantially lower cost, the full dataset yields negligible or no accuracy improvement (and occasionally slight degradation due to variance), so we conclude that 10% is a practical sweet spot for efficient pretraining on `commonsense-170k` dataset without sacrificing downstream performance.

Wall-clock time and memory consumption. With the same setup as described above, pretraining the projector on a 10% subset adds only about 10 minutes to the total fine-tuning time of roughly 5 hours for 3 epochs on a single NVIDIA H100 GPU, resulting in a runtime comparable to LoRA. In contrast, DoRA requires around 10 hours under the same configuration. Peak memory usage is dominated by the fine-tuning phase and remains similar across methods (82 GiB for LoRA and IPA, 81 GiB for DoRA). To fairly compare IPA and LoRA with similar computational budget, we also compared IPA (with 10%-data pretraining) to LoRA trained for 3% more steps, yielding average scores of 85.9 and 85.0 respectively, showing that the small pretraining cost consistently translates into a performance gain. Full ablation results are given in Appendix B.

Projected feature dimension. In our ablation study, we vary the hidden dimension d_h for IPA, LoRA, and DoRA, while keeping the learning rate, pretraining set size, and scaling ratio fixed. Figure 4a shows a characteristic bell-shaped curve for both IPA and LoRA: accuracy falls off steeply at very low dimensions, reaches a maximum over an intermediate range, then gradually declines as d_h increases further. Importantly, IPA is more robust than LoRA: at $d_h = 8$, it matches LoRA's performance at $d_h = 16$, whereas LoRA's accuracy drops sharply. DoRA maintains a relatively flat performance profile across all tested dimensions but underperforms IPA once $d_h \geq 8$. For intermediate dimensions ($d_h = 16, 32, 64$), LoRA still outperforms DoRA. Detailed per-task results are provided in Appendix B.

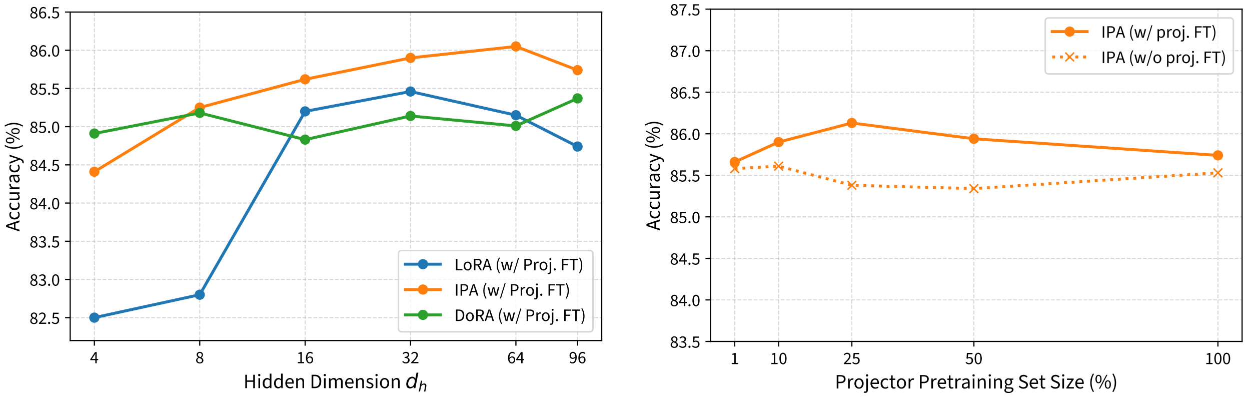

(a)

(b)

Figure 4: Average accuracy of Llama-3 8B models fine-tuned on commonsense benchmark with (a) varying hidden dimension d_h for IPA, compared to LoRA and DoRA, both with input projection fine-tuning ● ● ●, and (b) IPA (with projection fine-tuning ● or without ×) with varying percentage of the training dataset to obtain the projection pretraining feature set.

5 Discussion and Conclusion

In this paper, we presented the IPA framework, which addresses parameter-efficient adaptation by focusing on improving input-feature projection. We augment the feature projector with an input-feature-aware optimization objective, allowing it to learn meaningful projections without requiring gradient backpropagation. In our instantiation, we employ a batched PCA algorithm for unsupervised feature projection, demonstrating that this simple approach can be trained efficiently and effectively.

Through experiments on both language and vision-language benchmarks, we showed that IPA consistently outperforms existing PEFT methods that rely on random feature projections when the setting is aligned. These results confirm that incorporating data-driven projections yields more expressive and adaptable models while maintaining low additional parameter cost.

Future work could investigate alternative projection techniques, novel optimization objectives for the projector and the incorporation of other backpropagation-free unsupervised or self-supervised learning methods. Such enhancements may further boost adaptation performance while retaining the computational efficiency of our framework.

Acknowledgment

This work was granted access to the HPC resources of IDRIS under the allocation 2024-AD011015854 made by GENCI.

References

Paul Albert, Frederic Z. Zhang, Hemanth Saratchandran, Cristian Rodriguez Opazo, Anton van den Hengel, and Ehsan Abbasnejad. RandLoRA: Full rank parameter-efficient fine-tuning of large models. In *The Thirteenth International Conference on Learning Representations, ICLR 2025, Singapore, April 24-28, 2025*. OpenReview.net, 2025. URL https://openreview.net/forum?id=Hn5eoTunHN. 2, 3, 9

Rishi Bommasani, Drew A. Hudson, Ehsan Adeli, Russ Altman, Simran Arora, Sydney von Arx, Michael S. Bernstein, Jeannette Bohg, Antoine Bosselut, Emma Brunskill, Erik Brynjolfsson, Shyamal Buch, Dallas Card, Rodrigo Castellon, Niladri Chatterji et al. On the Opportunities and Risks of Foundation Models. *arXiv e-prints*, art. arXiv:2108.07258, August 2021. doi: 10.48550/arXiv.2108.07258. 1

Kerim Büyükakyüz. OLoRA: Orthonormal low-rank adaptation of large language models, 2024. URL https://arxiv.org/abs/2406.01775. 9

Hyung Won Chung, Le Hou, Shayne Longpre, Barret Zoph, Yi Tay, William Fedus, Yunxuan Li, Xuezhi Wang, Mostafa Dehghani, Siddhartha Brahma, Albert Webson, Shixiang Shane Gu, Zhuyun Dai, Mirac Suzgun, Xinyun Chen et al. Scaling instruction-finetuned language models. *J. Mach. Learn. Res.*, 25: 70:1–70:53, 2024. URL https://jmlr.org/papers/v25/23-0870.html. 4

Gemma Team, Aishwarya Kamath, Johan Ferret, Shreya Pathak, Nino Vieillard, Ramona Merhej, Sarah Perrin, Tatiana Matejovicova, Alexandre Ramé, Morgane Rivière, Louis Rouillard, Thomas Mesnard, Geoffrey Cideron, Jean-bastien Grill, Sabela Ramos et al. Gemma 3 Technical Report. *arXiv e-prints*, art. arXiv:2503.19786, March 2025. doi: 10.48550/arXiv.2503.19786. 6

Aaron Grattafiori, Abhimanyu Dubey, Abhinav Jauhri, Abhinav Pandey, Abhishek Kadian, Ahmad Al-Dahle, Aiesha Letman, Akhil Mathur, Alan Schelten, Alex Vaughan, Amy Yang, Angela Fan, Anirudh Goyal, Anthony Hartshorn, Aobo Yang et al. The Llama 3 Herd of Models. *arXiv e-prints*, art. arXiv:2407.21783, July 2024. doi: 10.48550/arXiv.2407.21783. 6

Demi Guo, Alexander M. Rush, and Yoon Kim. Parameter-efficient transfer learning with diff pruning. In Chengqing Zong, Fei Xia, Wenjie Li, and Roberto Navigli (eds.), *Proceedings of the 59th Annual Meeting of the Association for Computational Linguistics and the 11th International Joint Conference on Natural Language Processing, ACL/IJCNLP 2021, (Volume 1: Long Papers), Virtual Event, August 1-6, 2021*, pp. 4884–4896. Association for Computational Linguistics, 2021. doi: 10.18653/V1/2021.ACL-LONG.378. URL https://doi.org/10.18653/v1/2021.acl-long.378. 2

Zeyu Han, Chao Gao, Jinyang Liu, Jeff Zhang, and Sai Qian Zhang. Parameter-efficient fine-tuning for large models: A comprehensive survey. *Trans. Mach. Learn. Res.*, 2024, 2024. URL https://openreview.net/forum?id=lIsCS8b6zj. 1, 3

Soufiane Hayou, Nikhil Ghosh, and Bin Yu. The impact of initialization on LoRA finetuning dynamics. In Amir Globersons, Lester Mackey, Danielle Belgrave, Angela Fan, Ulrich Paquet, Jakub M. Tomczak, and Cheng Zhang (eds.), *Advances in Neural Information Processing Systems 38: Annual Conference on Neural Information Processing Systems 2024, NeurIPS 2024, Vancouver, BC, Canada, December 10 - 15, 2024*, 2024a. URL http://papers.nips.cc/paper_files/paper/2024/hash/d4387c37b3b06e55f86eccdb8cd1f829-Abstract-Conference.html. 3

Soufiane Hayou, Nikhil Ghosh, and Bin Yu. LoRA+: Efficient low rank adaptation of large models. In *Forty-first International Conference on Machine Learning, ICML 2024, Vienna, Austria, July 21-27, 2024*. OpenReview.net, 2024b. URL https://openreview.net/forum?id=NEv8YqBROO. 2, 3, 4

Junxian He, Chunting Zhou, Xuezhe Ma, Taylor Berg-Kirkpatrick, and Graham Neubig. Towards a unified view of parameter-efficient transfer learning. In *The Tenth International Conference on Learning Representations, ICLR 2022, Virtual Event, April 25-29, 2022*. OpenReview.net, 2022a. URL https://openreview.net/forum?id=0RDcd5Axok. 2

Shwai He, Liang Ding, Daize Dong, Jeremy Zhang, and Dacheng Tao. SparseAdapter: An easy approach for improving the parameter-efficiency of adapters. In Yoav Goldberg, Zornitsa Kozareva, and Yue Zhang (eds.), *Findings of the Association for Computational Linguistics: EMNLP 2022, Abu Dhabi, United Arab Emirates, December 7-11, 2022*, pp. 2184–2190. Association for Computational Linguistics, 2022b. doi: 10.18653/V1/2022.FINDINGS-EMNLP.160. URL https://doi.org/10.18653/v1/2022.findings-emnlp.160. 2

Harold Hotelling. Analysis of a complex of statistical variables into principal components. *J. Ed. Psych.*, 24: 417–441, 1933. 6

Neil Houlsby, Andrei Giurgiu, Stanislaw Jastrzebski, Bruna Morrone, Quentin de Laroussilhe, Andrea Gesmundo, Mona Attariyan, and Sylvain Gelly. Parameter-efficient transfer learning for NLP. In Kamalika Chaudhuri and Ruslan Salakhutdinov (eds.), *Proceedings of the 36th International Conference on Machine Learning, ICML 2019, 9-15 June 2019, Long Beach, California, USA*, volume 97 of *Proceedings of Machine Learning Research*, pp. 2790–2799. PMLR, 2019. URL http://proceedings.mlr.press/v97/houlsby19a.html. 1, 2

Edward J. Hu, Yelong Shen, Phillip Wallis, Zeyuan Allen-Zhu, Yuanzhi Li, Shean Wang, Lu Wang, and Weizhu Chen. LoRA: Low-rank adaptation of large language models. In *The Tenth International Conference on Learning Representations, ICLR 2022, Virtual Event, April 25-29, 2022*. OpenReview.net, 2022. URL https://openreview.net/forum?id=nZeVKeeFYf9. 1, 2, 7

Zhiqiang Hu, Lei Wang, Yihuai Lan, Wanyu Xu, Ee-Peng Lim, Lidong Bing, Xing Xu, Soujanya Poria, and Roy Ka-Wei Lee. LLM-Adapters: An adapter family for parameter-efficient fine-tuning of large language models. In Houda Bouamor, Juan Pino, and Kalika Bali (eds.), *Proceedings of the 2023 Conference on Empirical Methods in Natural Language Processing, EMNLP 2023, Singapore, December 6-10, 2023*, pp. 5254–5276. Association for Computational Linguistics, 2023. doi: 10.18653/V1/2023.EMNLP-MAIN.319. URL https://doi.org/10.18653/v1/2023.emnlp-main.319. 6, 7, 16

Chengsong Huang, Qian Liu, Bill Yuchen Lin, Tianyu Pang, Chao Du, and Min Lin. LoraHub: Efficient cross-task generalization via dynamic LoRA composition. *CoRR*, abs/2307.13269, 2023. doi: 10.48550/ARXIV.2307.13269. URL https://doi.org/10.48550/arXiv.2307.13269. 3

Qiushi Huang, Tom Ko, Zhan Zhuang, Lilian Tang, and Yu Zhang. HiRA: Parameter-efficient hadamard high-rank adaptation for large language models. In *The Thirteenth International Conference on Learning Representations, ICLR 2025, Singapore, April 24-28, 2025*. OpenReview.net, 2025. URL https://openreview.net/forum?id=TwJrTz9cRS. 2, 3

Shibo Jie, Haoqing Wang, and Zhi-Hong Deng. Revisiting the parameter efficiency of adapters from the perspective of precision redundancy. In *IEEE/CVF International Conference on Computer Vision, ICCV 2023, Paris, France, October 1-6, 2023*, pp. 17171–17180. IEEE, 2023. doi: 10.1109/ICCV51070.2023.01579. URL https://doi.org/10.1109/ICCV51070.2023.01579. 2

Diederik P. Kingma and Jimmy Ba. Adam: A method for stochastic optimization. In Yoshua Bengio and Yann LeCun (eds.), *3rd International Conference on Learning Representations, ICLR 2015, San Diego, CA, USA, May 7-9, 2015, Conference Track Proceedings*, 2015. URL http://arxiv.org/abs/1412.6980. 7

Dawid Jan Kopiczko, Tijmen Blankevoort, and Yuki M. Asano. VeRA: Vector-based random matrix adaptation. In *The Twelfth International Conference on Learning Representations, ICLR 2024, Vienna, Austria, May 7-11, 2024*. OpenReview.net, 2024. URL https://openreview.net/forum?id=NjNfLdxr3A. 2, 9

Minglei Li, Peng Ye, Yongqi Huang, Lin Zhang, Tao Chen, Tong He, Jiayuan Fan, and Wanli Ouyang. Adapter-X: A novel general parameter-efficient fine-tuning framework for vision. *CoRR*, abs/2406.03051, 2024. doi: 10.48550/ARXIV.2406.03051. URL https://doi.org/10.48550/arXiv.2406.03051. 2

Shih-Yang Liu, Chien-Yi Wang, Hongxu Yin, Pavlo Molchanov, Yu-Chiang Frank Wang, Kwang-Ting Cheng, and Min-Hung Chen. DoRA: Weight-decomposed low-rank adaptation. In *Forty-first International Conference on Machine Learning, ICML 2024, Vienna, Austria, July 21-27, 2024*. OpenReview.net, 2024. URL https://openreview.net/forum?id=3d5CIRG1n2. 2, 7, 16

Rabeeh Karimi Mahabadi, Sebastian Ruder, Mostafa Dehghani, and James Henderson. Parameter-efficient multi-task fine-tuning for transformers via shared hypernetworks. In Chengqing Zong, Fei Xia, Wenjie Li, and Roberto Navigli (eds.), *Proceedings of the 59th Annual Meeting of the Association for Computational Linguistics and the 11th International Joint Conference on Natural Language Processing, ACL/IJCNLP 2021, (Volume 1: Long Papers), Virtual Event, August 1-6, 2021*, pp. 565–576. Association for Computational Linguistics, 2021. doi: 10.18653/V1/2021.ACL-LONG.47. URL https://doi.org/10.18653/v1/2021.acl-long.47. 2

Yuren Mao, Yuhang Ge, Yijiang Fan, Wenyi Xu, Yu Mi, Zhonghao Hu, and Yunjun Gao. A survey on LoRA of large language models. *Frontiers Comput. Sci.*, 19(7):197605, 2025. doi: 10.1007/S11704-024-40663-9. URL https://doi.org/10.1007/s11704-024-40663-9. 3

Fanxu Meng, Zhaohui Wang, and Muhan Zhang. PiSSA: Principal singular values and singular vectors adaptation of large language models. In Amir Globersons, Lester Mackey, Danielle Belgrave, Angela Fan, Ulrich Paquet, Jakub M. Tomczak, and Cheng Zhang (eds.), *Advances in Neural Information Processing Systems 38: Annual Conference on Neural Information Processing Systems 2024, NeurIPS 2024, Vancouver, BC, Canada, December 10 - 15, 2024*, 2024. URL http://papers.nips.cc/paper_files/paper/2024/hash/db36f4d603cc9e3a2a5e10b93e6428f2-Abstract-Conference.html. 2, 9

Qwen, An Yang, Baosong Yang, Beichen Zhang, Binyuan Hui, Bo Zheng, Bowen Yu, Chengyuan Li, Dayiheng Liu, Fei Huang, Haoran Wei, Huan Lin, Jian Yang, Jianhong Tu, Jianwei Zhang et al. Qwen2.5 Technical Report. *arXiv e-prints*, art. arXiv:2412.15115, December 2024. doi: 10.48550/arXiv.2412.15115. 6

Sylvestre-Alvise Rebuffi, Hakan Bilen, and Andrea Vedaldi. Learning multiple visual domains with residual adapters. In Isabelle Guyon, Ulrike von Luxburg, Samy Bengio, Hanna M. Wallach, Rob Fergus, S. V. N. Vishwanathan, and Roman Garnett (eds.), *Advances in Neural Information Processing Systems 30: Annual Conference on Neural Information Processing Systems 2017, December 4-9, 2017, Long Beach, CA, USA*, pp. 506–516, 2017. URL https://proceedings.neurips.cc/paper/2017/hash/e7b24b112a44fdd9ee93bdf998c6ca0e-Abstract.html. 2

David A. Ross, Jongwoo Lim, Ruei-Sung Lin, and Ming-Hsuan Yang. Incremental learning for robust visual tracking. *Int. J. Comput. Vis.*, 77(1-3):125–141, 2008. doi: 10.1007/S11263-007-0075-7. URL https://doi.org/10.1007/s11263-007-0075-7. 6

Terence D. Sanger. Optimal unsupervised learning in a single-layer linear feedforward neural network. *Neural Networks*, 2(6):459–473, 1989. doi: 10.1016/0893-6080(89)90044-0. URL https://doi.org/10.1016/0893-6080(89)90044-0. 6

Reece Shuttleworth, Jacob Andreas, Antonio Torralba, and Pratyusha Sharma. LoRA vs full fine-tuning: An illusion of equivalence. *CoRR*, abs/2410.21228, 2024. doi: 10.48550/ARXIV.2410.21228. URL https://doi.org/10.48550/arXiv.2410.21228. 2

Yi-Lin Sung, Varun Nair, and Colin Raffel. Training neural networks with fixed sparse masks. In Marc'Aurelio Ranzato, Alina Beygelzimer, Yann N. Dauphin, Percy Liang, and Jennifer Wortman Vaughan (eds.), *Advances in Neural Information Processing Systems 34: Annual Conference on Neural Information Processing Systems 2021, NeurIPS 2021, December 6-14, 2021, virtual*, pp. 24193–24205, 2021. URL https://proceedings.neurips.cc/paper/2021/hash/cb2653f548f8709598e8b5156738cc51-Abstract.html. 2

Mirac Suzgun, Nathan Scales, Nathanael Schärli, Sebastian Gehrmann, Yi Tay, Hyung Won Chung, Aakanksha Chowdhery, Quoc V. Le, Ed H. Chi, Denny Zhou, and Jason Wei. Challenging BIG-Bench tasks and whether chain-of-thought can solve them. In Anna Rogers, Jordan L. Boyd-Graber, and Naoaki Okazaki (eds.), *Findings of the Association for Computational Linguistics: ACL 2023, Toronto, Canada, July 9-14, 2023*, pp. 13003–13051. Association for Computational Linguistics, 2023. doi: 10.18653/V1/2023.FINDINGS-ACL.824. URL https://doi.org/10.18653/v1/2023.findings-acl.824. 4

Pengwei Tang, Yong Liu, Dongjie Zhang, Xing Wu, and Debing Zhang. LoRA-Null: Low-rank adaptation via null space for large language models. *CoRR*, abs/2503.02659, 2025. doi: 10.48550/ARXIV.2503.02659. URL https://doi.org/10.48550/arXiv.2503.02659. 2

Chunlin Tian, Zhan Shi, Zhijiang Guo, Li Li, and Cheng-Zhong Xu. HydraLoRA: An asymmetric LoRA architecture for efficient fine-tuning. In Amir Globersons, Lester Mackey, Danielle Belgrave, Angela Fan, Ulrich Paquet, Jakub M. Tomczak, and Cheng Zhang (eds.), *Advances in Neural Information Processing Systems 38: Annual Conference on Neural Information Processing Systems 2024, NeurIPS 2024, Vancouver, BC, Canada, December 10 - 15, 2024*, 2024. URL http://papers.nips.cc/paper_files/paper/2024/hash/123fd8a56501194823c8e0dca00733df-Abstract-Conference.html. 2, 3, 4

Hugo Touvron, Louis Martin, Kevin Stone, Peter Albert, Amjad Almahairi, Yasmine Babaei, Nikolay Bashlykov, Soumya Batra, Prajjwal Bhargava, Shruti Bhosale, Dan Bikel, Lukas Blecher, Cristian Canton-Ferrer, Moya Chen, Guillem Cucurull et al. Llama 2: Open foundation and fine-tuned chat models. *CoRR*, abs/2307.09288, 2023. doi: 10.48550/ARXIV.2307.09288. URL https://doi.org/10.48550/arXiv.2307.09288. 6

Michael Tschannen, Alexey A. Gritsenko, Xiao Wang, Muhammad Ferjad Naeem, Ibrahim Alabdulmohsin, Nikhil Parthasarathy, Talfan Evans, Lucas Beyer, Ye Xia, Basil Mustafa, Olivier J. Hénaff, Jeremiah Harmsen, Andreas Steiner, and Xiaohua Zhai. SigLIP 2: Multilingual vision-language encoders with improved semantic understanding, localization, and dense features. *CoRR*, abs/2502.14786, 2025. doi: 10.48550/ARXIV.2502.14786. URL https://doi.org/10.48550/arXiv.2502.14786. 6

Xujia Wang, Haiyan Zhao, Shuo Wang, Hanqing Wang, and Zhiyuan Liu. MALoRA: Mixture of asymmetric low-rank adaptation for enhanced multi-task learning. In Luis Chiruzzo, Alan Ritter, and Lu Wang (eds.), *Findings of the Association for Computational Linguistics: NAACL 2025, Albuquerque, New Mexico, USA, April 29 - May 4, 2025*, pp. 5609–5626. Association for Computational Linguistics, 2025. doi: 10.18653/V1/2025.FINDINGS-NAACL.312. URL https://doi.org/10.18653/v1/2025.findings-naacl.312. 3

Yibo Yang, Xiaojie Li, Zhongzhu Zhou, Shuaiwen Song, Jianlong Wu, Liqiang Nie, and Bernard Ghanem. CorDA: Context-oriented decomposition adaptation of large language models for task-aware parameter-efficient fine-tuning. In Amir Globersons, Lester Mackey, Danielle Belgrave, Angela Fan, Ulrich Paquet, Jakub M. Tomczak, and Cheng Zhang (eds.), *Advances in Neural Information Processing Systems 38: Annual Conference on Neural Information Processing Systems 2024, NeurIPS 2024, Vancouver, BC, Canada, December 10 - 15, 2024*, 2024. URL http://papers.nips.cc/paper_files/paper/2024/hash/83f95bb0ac5046338ea2afe3390e9f4b-Abstract-Conference.html. 2, 9

Xiaohua Zhai, Joan Puigcerver, Alexander Kolesnikov, Pierre Ruyssen, Carlos Riquelme, Mario Lucic, Josip Djolonga, André Susano Pinto, Maxim Neumann, Alexey Dosovitskiy, Lucas Beyer, Olivier Bachem, Michael Tschannen, Marcin Michalski, Olivier Bousquet et al. The visual task adaptation benchmark. *CoRR*, abs/1910.04867, 2019. URL http://arxiv.org/abs/1910.04867. 6

Dan Zhang, Tao Feng, Lilong Xue, Yuandong Wang, Yuxiao Dong, and Jie Tang. Parameter-Efficient Fine-Tuning for Foundation Models. *arXiv e-prints*, art. arXiv:2501.13787, January 2025. doi: 10.48550/arXiv.2501.13787. 1

Yuanhan Zhang, Kaiyang Zhou, and Ziwei Liu. Neural prompt search. *CoRR*, abs/2206.04673, 2022. doi: 10.48550/ARXIV.2206.04673. URL https://doi.org/10.48550/arXiv.2206.04673. 6, 7

Yuanhe Zhang, Fanghui Liu, and Yudong Chen. LoRA-One: One-step full gradient could suffice for fine-tuning large language models, provably and efficiently. In *Forty-second International Conference on Machine Learning*, 2025. URL https://openreview.net/forum?id=KwIlvmLDLm. 4

Jiacheng Zhu, Kristjan H. Greenewald, Kimia Nadjahi, Haitz Sáez de Ocáriz Borde, Rickard Brüel Gabrielsson, Leshem Choshen, Marzyeh Ghassemi, Mikhail Yurochkin, and Justin Solomon. Asymmetry in low-rank adapters of foundation models. In *Forty-first International Conference on Machine Learning, ICML 2024, Vienna, Austria, July 21-27, 2024*. OpenReview.net, 2024. URL https://openreview.net/forum?id=txRZBD8tBV. 2, 3, 4

A Experimental Detail

Hyperparameters. The hyperparameters used across all models are summarized as follows. For instruction-following tasks, we adopt a batch size of 16, aligning with Hu et al. (2023) and Liu et al. (2024). For open-vocabulary image classification, we use a batch size of 64.

We use a learning rate of 3×10^{-4} for Llama-2 7B, and 1×10^{-4} for Llama-3 8B, Qwen-2.5 7B, and Gemma-3 4B. For all, LoRA and DoRA use a scaling factor ($\lambda = \frac{\alpha}{d_h}$) of 2, while IPA uses 0.25, except for Gemma-3 4B, where it is 0.4. For SigLIP 2, we apply a learning rate of 1×10^{-3}, scaling factors of 2 (LoRA/DoRA) and 0.5 (IPA), with a dropout rate of 0.1 across all variants.

B Additional Illustration and Experimental Results

Feature-wise similarity. To complement the global similarity shown in Figure 1a through the cosine similarity of LoRA's A matrices with respect to their initialization, we present in Figure 5 a comparison based on feature-wise similarity. We compute the expected cosine similarity of the projected features as follows: using the pretraining features $\hat{x}$ introduced in Section 3.4, we calculate, for each task j, the cosine similarity across the layers Λ where LoRA is applied:

$$\frac{\sum_{\ell\in\Lambda}\sum_{\hat{x}^{(\ell)}}\left((A_0^{(\ell)}\hat{x}^{(\ell)})^\top A_{T,j}^{(\ell)}\hat{x}^{(\ell)}\right)}{\sqrt{\sum_{\ell\in\Lambda}\sum_{\hat{x}^{(\ell)}}\left((A_0^{(\ell)}\hat{x}^{(\ell)})^\top A_0^{(\ell)}\hat{x}^{(\ell)}\right)}\sqrt{\sum_{\ell\in\Lambda}\sum_{\hat{x}^{(\ell)}}\left((A_{T,j}^{(\ell)}\hat{x}^{(\ell)})^\top A_{T,j}^{(\ell)}\hat{x}^{(\ell)}\right)}}.$$

On average, the projected features remain moderately similar to the original projected features across tasks.

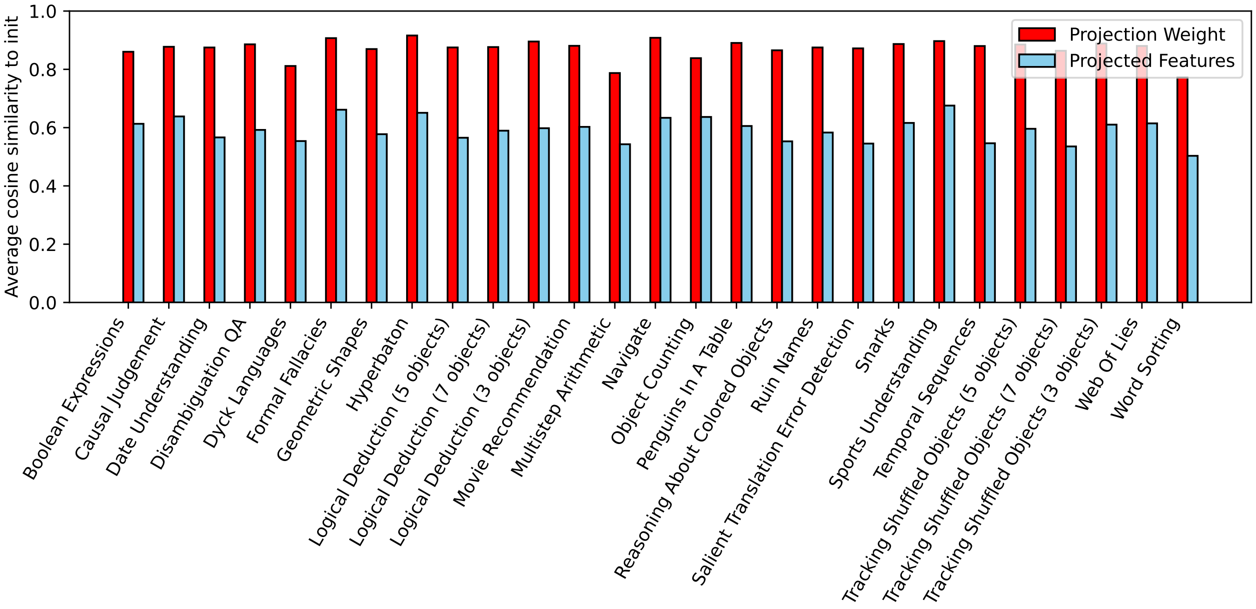

Figure 5: **Cosine similarity of LoRA A projections after fine-tuning on 27 BBH tasks, compared to the initial projection, versus the similarity of projected features.** To capture the local behavior of the projection, we complement Figure 1a with a measure of feature-wise similarity between the projected representations.

Detailed results of additional baselines. Table 6 reports the full per-task results for the extended set of baselines introduced in Table 3.

Method	Learning Rate	BoolQ	PIQA	SocialIQA	HellaSwag	WinoGrande	ARC-easy	ARC-challenge	OpenbookQA	Avg.
LoRA	1×10^{-4}	75.4	88.6	80.7	95.4	86.2	91.2	80.1	86.1	85.5
DoRA	1×10^{-4}	75.3	89.3	80.8	95.3	85.8	89.9	79.3	85.6	85.1
PiSSA	2×10^{-5}	75.2	88.6	81.1	94.8	85.5	89.8	77.1	84.6	84.6
OLoRA	2×10^{-5}	73.9	87.6	79.3	94.7	84.9	90.0	79.4	85.0	84.4
CorDA	2×10^{-5}	71.6	85.0	77.0	91.6	82.6	85.4	72.0	81.4	80.8
RandLoRA	1×10^{-4}	72.0	86.8	79.7	94.6	85.2	89.3	77.0	82.8	83.4
VeRA (r=512)	4×10^{-3}	62.2	85.2	77.8	91.7	80.3	87.2	75.2	81.6	80.1
IPA	1×10^{-4}	75.0	89.9	81.2	96.0	85.9	91.2	79.6	88.4	85.9

Table 6: Detailed results on comparison of with additional PEFT methods.

Projection	Proj. FT	Scaling	BoolQ	PIQA	SocialIQA	HellaSwag	WinoGrande	ARC-easy	ARC-challenge	OpenbookQA	Avg.
Random ortho.	✗	0.25	62.5	85.9	79.3	93.3	82.7	89.6	78.2	82.2	81.7
Random ortho.		$0.25\sqrt{\frac{d_{\text{in}}}{d_{\text{h}}}}$	65.9	86.9	79.5	94.1	84.1	89.1	75.8	81.6	82.2
LoRA		$\alpha/r = 2$	73.6	88.1	80.3	95.0	85.2	90.4	80.1	87.4	85.0
IPA (Ours)		0.25	74.8	88.6	81.1	95.4	85.6	91.7	79.9	87.8	85.6
Random ortho.	✓	0.25	75.1	88.8	81.5	95.60	86.1	90.5	80.0	86.8	85.5
Random ortho.		$0.25\sqrt{\frac{d_{\text{in}}}{d_{\text{h}}}}$	63.3	87.3	80.5	94.0	85.2	90.0	78.8	85.8	83.1
LoRA		$\alpha/r = 2$	75.4	88.6	80.7	95.4	86.2	91.2	80.1	86.1	85.5
IPA (Ours)		0.25	75.0	89.9	81.2	96.0	85.9	91.2	79.6	88.4	85.9

Table 7: Comparison of projection types on commonsense.

Detailed results of ablation study. Tables 8 and 9 show the detailed results of the ablation studies in Figures 4a and 4b in Section 4.4. Table 10 shows the detailed results on the ablation study about compute budget in Section 4.4.

Table 8: Detailed results of the ablation study on different hidden dimensions.

Method	Proj. FT	Hidden Dim.	BoolQ	PIQA	SocialIQA	HellaSwag	WinoGrande	ARC-easy	ARC-challenge	OpenbookQA	Avg.
LoRA	✓	4	62.1	87.9	78.9	91.3	84.0	89.9	79.4	86.6	82.5
		8	62.1	88.8	80.5	92.3	83.0	90.2	80.7	84.8	82.8
		16	74.7	87.4	80.9	95.4	86.7	90.0	79.4	87.2	85.2
		32	75.4	88.6	80.7	95.4	86.2	91.2	80.1	86.1	85.5
		64	75.1	88.4	81.0	93.0	86.9	90.4	79.7	86.8	85.1
		96	74.9	88.4	79.8	94.6	86.3	89.6	78.8	85.4	84.7
DoRA	✓	4	73.6	88.6	79.8	95.5	85.1	90.2	80.3	86.2	84.9
		8	75.6	89.1	80.7	95.6	85.2	90.9	78.7	85.8	85.2
		16	73.5	88.9	80.2	95.3	86.1	90.5	78.6	85.6	84.8
		32	75.3	89.3	80.8	95.3	85.8	89.9	79.3	85.6	85.1
		64	74.8	88.6	80.9	94.9	85.3	89.4	79.9	86.2	85.0
		96	74.6	89.0	80.0	95.3	85.9	90.4	79.0	88.8	85.4
IPA	✓	4	73.7	88.0	79.2	95.0	84.0	89.9	79.7	85.8	84.4
		8	73.7	89.0	81.1	95.6	86.3	91.0	80.1	85.2	85.2
		16	74.6	88.9	80.6	96.0	85.1	91.0	80.3	88.6	85.6
		32	75.0	89.9	81.2	96.0	85.9	91.2	79.6	88.4	85.9
		64	75.9	88.4	80.4	95.9	87.5	91.5	81.0	87.8	86.1
		96	75.6	88.2	81.4	95.9	86.6	91.0	80.5	86.8	85.7

Table 9: Detailed results of the ablation study on projector pretraining set size.

Method	Proj. FT	Proj. Pretraining Set	BoolQ	PIQA	SocialIQA	HellaSwag	WinoGrande	ARC-easy	ARC-challenge	OpenbookQA	Avg.
IPA	✗	1%	74.1	88.5	80.9	95.3	86.1	91.4	80.8	87.6	85.6
		10%	74.9	88.5	81.0	95.7	85.6	91.0	80.0	88.2	85.6
		25%	73.6	88.2	80.5	95.5	85.8	91.0	80.1	88.4	85.4
		50%	74.3	88.2	80.7	95.3	85.4	90.2	80.4	88.2	85.3
		100%	73.7	88.0	81.1	95.2	86.6	90.7	80.1	88.8	85.5
	✓	1%	75.2	88.8	81.0	95.6	86.5	91.3	79.6	87.2	85.7
		10%	75.0	89.9	81.2	96.0	85.9	91.2	79.6	88.4	85.9
		25%	75.4	89.4	81.8	96.0	88.1	91.1	79.9	87.4	86.1
		50%	74.9	89.2	81.5	95.9	87.6	91.1	80.7	86.6	85.9
		100%	75.1	88.8	80.8	96.1	86.9	90.9	79.9	87.6	85.7

Table 10: Comparison between LoRA and IPA under matched computational budgets. LoRA is trained for about 3% more steps to match total training time of IPA pretrained with 10% of training data.

Method	Proj. FT	FT Steps	BoolQ	PIQA	SocialIQA	HellaSwag	WinoGrande	ARC-easy	ARC-challenge	OpenbookQA	Avg.
LoRA	✓	32,887	76.2	88.0	80.1	95.0	86.7	90.6	78.5	84.4	85.0
IPA	✓	31,926	75.0	89.9	81.2	96.0	85.9	91.2	79.6	88.4	85.9